
Flew Over Learning Trap: Learn Unlearnable Samples by Progressive Staged Training

Pucheng Dang^{1,2} Xing Hu^{2,4} * Kaidi Xu³ Jinhao Duan³ Di Huang^{1,2}
 Husheng Han^{1,2} Rui Zhang² Zidong Du^{2,4} Qi Guo² Yunji Chen^{1,2}

¹ University of Chinese Academy of Sciences, China

² State Key Lab of Processors, Institute of Computing Technology,
 Chinese Academy of Sciences, Beijing, China

³ Drexel University

⁴ Shanghai Innovation Center for Processor Technologies, SHIC
 {dangpucheng20g,huxing,hanhusheng20z,huangdi20b}@ict.ac.cn
 {zhangrui,duzidong,guoqi,cyj}@ict.ac.cn
 {kx46,jd3734}@drexel.edu

Abstract

Unlearning techniques are proposed to prevent third parties from exploiting unauthorized data, which generate unlearnable samples by adding imperceptible perturbations to data for public publishing. These unlearnable samples effectively misguide model training to learn perturbation features but ignore image semantic features. We make the in-depth analysis and observe that models can learn both image features and perturbation features of unlearnable samples at an early stage, but rapidly go to the overfitting stage since the shallow layers tend to overfit on perturbation features and make models fall into overfitting quickly. Based on the observations, we propose *Progressive Staged Training* to effectively prevent models from overfitting in learning perturbation features. We evaluated our method on multiple model architectures over diverse datasets, e.g., CIFAR-10, CIFAR-100, and ImageNet-mini. Our method circumvents the unlearnability of all state-of-the-art methods in the literature and provides a reliable baseline for further evaluation of unlearnable techniques. The code is available at <https://github.com/CherryBlueberry/ST>.

1 Introduction

Deep neural networks (DNNs) significantly boost computer vision techniques in the past decade and achieve even better capabilities surpassing human beings. One of the most important factors contributing to the great success comes from the representative and valuable data collected for training. Not only influential public datasets such as CIFAR [10] and ImageNet [17] are proposed for benchmark evaluation, but also huge volumes of scenario-sensitive data are used for real model training and deployment [21; 15]. Data has become one type of important asset and it is crucial to ensure authorized access to sensitive data.

Previous studies propose “unlearnable sample” techniques aiming to address the issue of unauthorized access to sensitive data [9; 6; 26; 16; 24]. The unlearnable samples are produced by injecting carefully-crafted imperceptible perturbations into the training data, which induce models to learn the meaningless perturbation features instead of the valuable semantic features of nature images. Error-minimizing (EM) [9] perturbations are produced by an alternating bi-level min-min optimization on

*Corresponding author

both model parameters and perturbations. However, EM perturbations have no defense on adversarial training which adds perturbations to input while training to improve the robustness of models. To solve this problem robust error-minimizing (REM) [6] perturbations implement adversarial training while generating unlearnable perturbations, which grants perturbations the ability to resist adversarial training. [26] found that perturbations act as shortcuts to mislead models to a bad state, and proposed synthetic perturbations (SP) which generate unlearnable perturbations without the optimization of error-minimization. In order to improve the transferability of unlearnable perturbations, [16] proposed transferable unlearnable samples which protects data privacy from unsupervised learning. One-pixel shortcut (OPS) [24] used a perceptible pixel as the perturbation to protect data. The state-of-the-art study [24] show good protection that lowers the learning accuracy from 92.41% to 21.71% of ResNet-18 on CIFAR-10.

In this work, we differentiate features learned from unlearnable samples and nature samples and propose powerful defeat techniques to break the protection from superior unlearnable perturbation generators effectively. The analysis sheds light on data property protection and urges new protection mechanisms. There are two kinds of features in unlearnable samples: perturbation features and image semantic features. The former achieves serious overfitting, and the latter validly generalizes to test data (Fig. 1). Specifically, we make the following observations: 1) Model training at the early stage learns both the perturbation features and image semantic features. Then the model quickly overfits to learn the perturbation features only in the subsequent learning processes. 2) Shallow layers tend to overfit on perturbation features and make the models fall into overfitting quickly. When shallow layers are overfitting, undesirable activation will pass through the shallow layers and corrupt deep layers in an overfitting way. The intrinsic reasons behind this phenomenon are that unlearnable perturbation set up “fake” and simple features, and model prefers these features rather than image semantic features because that the former is easier to optimize the learning objective.

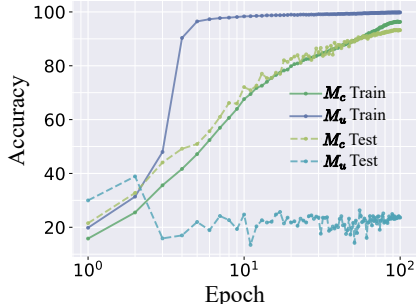


Figure 1: The training and test accuracy of a ResNet-18 trained on clean data (M_c) and unlearnable data (M_u).

Based on the observations, we show insights that models have the ability to learn valid semantic features from unlearnable samples at the early training stage, and stopping the overfitting of shallow layers extremely contribute to stopping the overfitting of the whole model. In this case, we propose a training framework, progressive staged training (ST), to effectively prevent models from overfitting in learning perturbation features. ST estimates whether the models are in an overfitting state and trains models with a progressive staged strategy of learning rate adjustment. To quantitatively evaluate whether the model is in an overfitting state, we propose Activation Cluster Measurement (*ACM*), based on the insight that perturbation features have a larger inter-class distance and smaller intra-class distance [26] in a low dimension space. To demonstrate the efficacy of ST, we conduct comprehensive experiments with multiple model architectures on CIFAR-10, CIFAR-100, and ImageNet-mini. Experimental results show that ST significantly defeats existing unlearnable techniques and provides a reliable baseline for further evaluation of unlearnable samples.

We summarize our contributions as follows:

- We show insights that models are capable of learning valid image semantic features from unlearnable samples at the early stage of training. Preventing overfitting in shallow layers significantly contributes to mitigating overfitting in the entire model.
- We propose a learning framework, ST, to prevent models from being overfitted to the features forged by unlearnable perturbations, with the help of *ACM* metric for quantitatively evaluating whether the model is in the overfitting state.
- We perform comprehensive experiments to show that our ST framework break all state-of-the-art unlearning samples in literatures on multiple model architectures across various datasets.

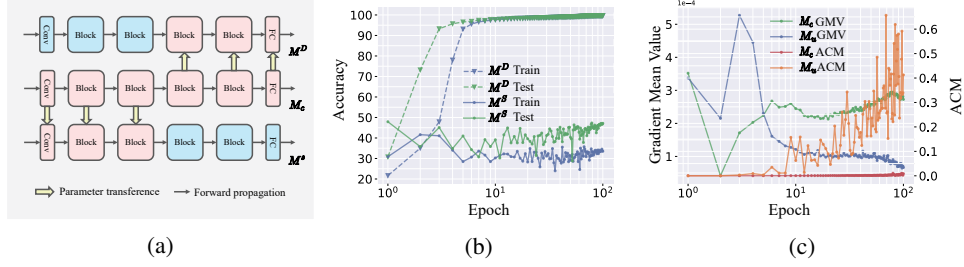


Figure 2: (a) The sketch of M^S and M^D . (b) The training accuracy and test accuracy of M^S (green) and M^D (blue) on unlearnable data. (c) The mean value of gradient (GMV) and ACM at each epoch of a shallow layer when trained on clean data M_c and unlearnable data M_u .

2 Related work

Data Poisoning Attack. Data poisoning involves altering the training data in order to negatively impact the performance of models. Typically, the modified, poisoned examples only make up a portion of the entire dataset, and are easily identifiable as being notably modified [1; 25; 18; 5].

Unlearnable Sample. As a special case of poison attack, unlearnable sample [9; 6; 26; 16; 24] shares similar mechanisms of data poisoning attacks. However, unlearnable sample is a kind of data protection method that adds imperceptible perturbations to the entire dataset. Suppose that $\{(\mathbf{x}_i, \mathbf{y}_i)\}_{i=1}^n$ is the training dataset with the input data $\mathbf{x}_i \in \mathbf{X}$ and the associated label $\mathbf{y}_i \in \mathbf{Y} = \{1, 2, \dots, k\}$. We assume that the unauthorized parties will use the published training dataset to train a classifier $f_\theta : \mathbf{X} \rightarrow \mathbf{Y}$ with parameter θ . Error-minimizing (EM) [9] perturbations are produced by an alternating bi-level min-min optimization on both model parameters and perturbations:

$$\arg \min_{\theta} \mathbb{E}_{(\mathbf{x}_i, \mathbf{y}_i)} \left[\min_{\delta_i} \mathcal{L}(f_\theta(\mathbf{x}_i + \delta_i), \mathbf{y}_i) \right] \quad (1)$$

where \mathcal{L} is the cross entropy loss and $\|\delta_i\|_\infty < \epsilon$. Being induced to trust that the perturbation can minimize the loss better than the original image features, the model will pay more attention to the perturbations. However, EM perturbations have no defense on adversarial training which adds random perturbations to input while training to improve the robustness of models. To solve this problem robust error-minimizing (REM) [6] perturbations implement adversarial training while generating unlearnable perturbations, which grants perturbations the ability to resist adversarial training:

$$\arg \min_{\theta} \mathbb{E}_{(\mathbf{x}_i, \mathbf{y}_i)} \left[\min_{\delta_i} \max_{\sigma_i} \mathcal{L}(f_\theta(\mathbf{x}_i + \delta_i + \sigma_i), \mathbf{y}_i) \right] \quad (2)$$

where $\|\sigma_i\|_\infty < \epsilon_a$ and $\|\delta_i\|_\infty < \epsilon_u$. Yu, et al. found that perturbations act as shortcuts to mislead models to a bad state, and proposed synthetic perturbations (SP) [26] which generates unlearnable perturbations without the optimization of error-minimization. In order to improve the transferability of unlearnable perturbations, Ren, et al. proposed transferable unlearnable samples [16], which protects data privacy from unsupervised learning. One-pixel shortcut (OPS) [24] used a perceptible pixel as perturbations to protect data.

3 Method

We first expose the observations on the training process over unlearnable samples and propose two insights on the learning process of models trained on unlearnable samples (Sec. 3.1). Then, based on these insights, we propose progressive staged training (ST), the first effective training framework to make unlearnable samples learnable. We further propose Activation Cluster Measurement (ACM), an indicator to identify whether or not the entire model is overfitting. We also investigate a special color space transformation (color-jitter and gray-scale) that promotes the performance of ST. The overall pipeline of ST to defeat unlearnable samples is presented in Sec. 3.2.

3.1 Insights

*Insight 1: Model learns both image semantic feature and perturbation features at the **early** stage before being trapped in the overfitting status, which provides a "golden window" for image features*

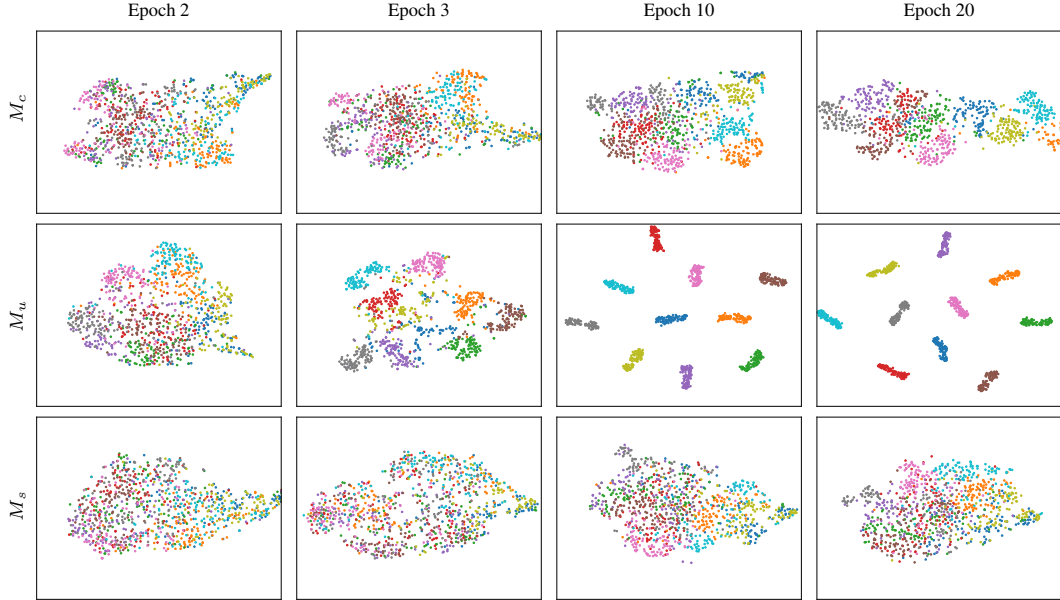


Figure 3: The penultimate layer activation t-SNE results of various models in different epochs. M_c is a model natural trained on clean data. M_u is a model natural trained on unlearnable data. M_s is a model ST trained on unlearnable data. Both the x-axis and the y-axis are in the range of $[-50, 50]$.

learning. To demonstrate this insight, we show the learning process of a ResNet-18 on unlearnable CIFAR-10 in Fig. 1 (more results of other models and datasets can be found in Appendix Sec. B.1). It is shown that both the training accuracy and test accuracy increase at the first several epochs, indicating that the model learned valid image semantic features. However, after epoch 3, the training accuracy increases sharply, while the test accuracy significantly decreases, indicating the model is overfitting and trapped in the unlearnable perturbation features learning. In summary, a model is capable of learning the valid semantic features from unlearnable examples at the early stage of training. Then, the model will learn more perturbations features than valid image semantic features as the training going, which gets trapped by unlearnable samples eventually.

Although there are several methods to prevent models from overfitting in natural training [20; 11; 4; 29; 27; 2; 3], these methods do not consider such stronger unlearnable perturbations and perform poorly on defeating unlearnable samples (Sec. 4.2). In this work, we take the model learning gap between image semantic features and perturbation features into consideration and train the model under the monitoring of an overfitting indicator to prevent it from being trapped.

Insight 2: Perturbation features tend to overfit shallow layers rather than deep layers because the prior can trap the models easily. To show that, we first trained a ResNet-18 [7] model on clean CIFAR-10 [10] denoted by M_c , which achieves 92.41% accuracy on CIFAR-10 test data. We randomly initialized a ResNet-18 and replaced the first two residual blocks with the first two residual blocks of M_c . Then we froze these replaced blocks' parameters and denoted this ResNet-18 by M^S . Similarly, we randomly initialized another ResNet-18 and replaced the last two residual blocks with the last two residual blocks of M_c . Then we froze these replaced blocks' parameters and denoted this ResNet18 by M^D (details in Fig. 2 (a) and more results of other models and datasets can be found in Appendix Sec. B.2). Finally, we trained M^S and M^D on CIFAR-10 unlearnable data individually. Training results are presented in Fig. 2 (b). It is shown that M^S performs better on CIFAR-10 test data, which proves that shallow layers are capable of learning the correct features at the beginning of the training (like M^S). However, when shallow layers are overfitting, even if deep layers are in the right state (like M^D), shallow layers will pass the wrong activation and corrupt the model to an overfitting way. In this case, how to prevent shallow layers from overfitting is crucial to break unlearnable samples' data protective ability. This phenomenon inspired us to propose a progressive staged training strategy that adjusts the learning rate to slow down the learning process of shallow layers gradually to avoid overfitting.

3.2 ST Training Framework

With the insights above, we propose progressive staged training (ST), a progressive staged training strategy by gradually modifying the learning rate of different layers from shallow layers to deep layers when the model has the tendency to overfit. To decide when to modify the learning rate of layers, we propose the Activation Cluster Measurement (ACM) as an indicator to detect the tendency of overfitting caused by unlearnable perturbations during the training period. Meanwhile, a novel learning rate schedule algorithm is proposed to gradually reduce the learning process of shallow layers to resist overfitting.

Overfitting Indicator. We propose a metric to quantitatively estimate whether the model is in a perturbation overfitting state, based on the observation that unlearnable perturbations construct simple features, and models are recognized to be “lazy” and prefer to learn simple unlearnable perturbation features rather than difficult image semantic features [26].

To make the above analysis clear and visualized, we present the t-SNE [23] clustering results of the penultimate layer activation at different training epochs. As shown in Fig. 3, when a model is trained on unlearnable samples, the activation cluster disorder at early epochs, i.e., the intra-class distance is large and inter-class distance is small. As training goes on, the activation begins to cluster well (a small intra-class distance and a large inter-class distance), which is a phenomenon of overfitting (other t-SNE results can be found in Appendix Sec. C.6). The visualization results of t-SNE also reflect the overfitting during training. To quantify this phenomenon, we propose a clustering measure named Activation Cluster Measurement (ACM) to describe the disorder of activation in different training epochs. Suppose that $D = \{D_i\}_{i=1}^k$ is a dataset with k labels, and D_i is the set of samples in class i . We define set A_i^M as the penultimate layer activation of model M when given it with set D_i as inputs. The cluster center of class i is defined as $C(i) = \frac{1}{|A_i^M|} \sum_{\mathbf{x} \in A_i^M} \mathbf{x}$. Then we have the intra-class distance σ for class i as:

$$\sigma(i) = \frac{1}{|A_i^M|} \sum_{\mathbf{x} \in A_i^M} \|\mathbf{x} - C(i)\|_2 \quad (3)$$

And the inter-class distance L between class i and j is as follows:

$$L(i, j) = \min \{\|\mathbf{x} - \mathbf{y}\|_2\}_{\mathbf{x} \in A_i^M, \mathbf{y} \in A_j^M} \quad (4)$$

Then we define ACM of model M on dataset D as:

$$ACM(M, D) = \frac{1}{k(k-1)} \sum_{\substack{i, j=1 \\ i \neq j}}^k \frac{L(i, j)}{R(i)\sigma(i) + R(j)\sigma(j)} \quad (5)$$

where k is the number of classes. $R(i)$ is the radius of class i : $R(i) = \max \{\|\mathbf{x} - C(i)\|_2\}_{\mathbf{x} \in A_i^M}$. The ACM of the model trained on clean data (M_c) and unlearnable data (M_u) at different training epochs is shown in Fig. 2 (c). We use D_s , a subset of the training dataset, as the validation set to calculate ACM metric during staged training (details in 4.1). The ACM of the M_u is low at the beginning, then it goes to a high level, which is consistent with our previous observation in Fig. 3 that the inter-class distance becomes larger and intra-class distance becomes smaller. Meanwhile, The gradient mean value (GMV) of the model trained on unlearnable data falls down to a low level, which illustrates that shallow layers are trapped in overfitting status and hardly learn new knowledge at late epochs compared to the model trained on clean data.

Progressive Staged Training. Based on the observations above, we propose progressive staged training (ST), a novel stage training framework to defeat unlearnable samples. For a given model M with l layers and a dataset D , the natural training (NT) process goes through three steps traditionally in each epoch: learning rate attenuation, forward propagation, and back propagation. Differently, ST goes through five steps in each epoch: learning rate attenuation, learning rate adjustment, forward propagation, back

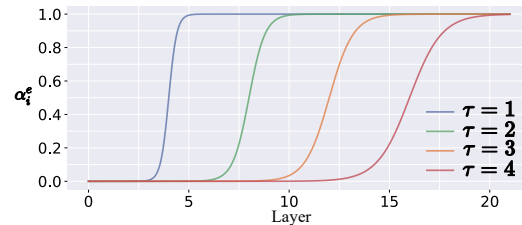


Figure 4: Different τ^e value for α_i^e in Eq. 7 with $\beta = \frac{1}{5}$, $l = 20$.

Algorithm 1 Staged Training (ST)

Input: dataset D , model $f_{\theta} = \{f_{\theta_1}, f_{\theta_2}, \dots, f_{\theta_l}\}$, small data D^s , threshold γ , hyperparameter β , epoch number E , learning rate η , attenuation function $Atten$
Initialize $\tau_e \leftarrow 0$, $\hat{\eta}_i^0 \leftarrow \eta$, $\mathbf{H}^{tmp} \leftarrow \mathbf{H}^0 \leftarrow [\alpha_1^0, \alpha_2^0, \dots, \alpha_l^0] \leftarrow [1, 1, \dots, 1]$, $\theta^{tmp} \leftarrow \theta$
for $e = 1$ **to** E **do**
 $\hat{\eta}_i^e \leftarrow Atten(\hat{\eta}_i^{e-1})$, $\eta_i^e \leftarrow \alpha_i^e \cdot \hat{\eta}_i^e$ ▷ learning rate attenuation and adjustment
 $\theta_i \leftarrow Train(\eta_i^e, D)$ ▷ optimize $\theta = \{\theta_1, \theta_2, \dots, \theta_l\}$ using back propagation
 Calculate $ACM(f_{\theta}, D^s)$ by Eq. (5)
 if $ACM(f_{\theta}, D^s) > \gamma$ and $\tau_e < \frac{1}{\beta} - 1$ **then** ▷ model tends to overfitting
 $\tau_e \leftarrow \tau_e + 1$
 $\theta \leftarrow \theta^{tmp}$ ▷ load checkpoint from θ^{tmp}
 Calculate α_i^e by Eq. (7)
 $\mathbf{H}^e \leftarrow [\alpha_1^e, \alpha_2^e, \dots, \alpha_l^e]$ ▷ using \mathbf{H}^e to adjust learning rate in next epoch
 ▷ model does not tend to overfitting
 else
 if $\tau_e = 0$ **then**
 $\mathbf{H}^e \leftarrow [1, 1, \dots, 1]$ ▷ natural training in next epoch
 else
 $\mathbf{H}^e \leftarrow \mathbf{H}^{tmp}$ ▷ using \mathbf{H}^{tmp} to adjust learning rate in next epoch
 end if
 $\theta^{tmp} \leftarrow \theta$ ▷ save checkpoint to θ^{tmp}
 end if
 $\mathbf{H}^{tmp} \leftarrow \mathbf{H}^e$
end for

propagation and ACM calculation. Once ACM indicates overfitting at the end of an epoch, the model will roll back to the checkpoint of the last epoch. Then, the learning rate will be further modified by an adjustment algorithm after learning rate attenuation to slow down the learning process of shallow layers gradually to resist overfitting. Suppose the initial learning rate of the i th layer of model M is $\hat{\eta}_i^0$ and $Atten$ is a learning rate attenuation function like momentum [22], cosine [14], etc. In every epoch, we first get an attenuated learning rate $\hat{\eta}_i^e = Atten(\hat{\eta}_i^{e-1})$, e for the e -th epoch. Then we get a new learning rate η_i^e by adjusting $\hat{\eta}_i^e$ with α_i^e (i for the i -th layer) as follows.

$$\eta_i^e = \alpha_i^e \cdot \hat{\eta}_i^e \quad (6)$$

$$\alpha_i^e = 1 - \frac{1}{1 + e^{\frac{i}{\beta \cdot \tau_e} - 1}} \quad (7)$$

where τ_e is a counter for how many time ACM larger than a threshold γ from the beginning to epoch e and β is a hyperparameter. We use a vector $\mathbf{H}^e = [\alpha_1^e, \alpha_2^e, \dots, \alpha_l^e]$ to describe how the learning rate adjustment algorithm works and defeat overfitting as shown in Fig. 4. At the beginning of training, we set $\mathbf{H}^0 = [1, 1, \dots, 1]$, which is equivalent to natural training, and all layers have the same learning rate. As the training goes on, the model tends to overfit and the count τ_e is increased. Meanwhile, following the components of \mathbf{H} , the learning rate of each layer gradually decreased to zero, which means the optimization gradually slow down from shallow layers to deep layers to resist overfitting. The process of ST is described in Alg. 1.

ST Training Pipeline. We also investigate that some data augmentations, e.g., color-jitter and gray-scale (CG) [12], could promote the performance of ST. Color-jitter randomly changes the brightness, contrast, saturation, and hue of an image. Gray-scale randomly converts an image to grayscale. We analyze that CG makes unlearnable perturbations harder to learn for models and weaker on data protection, even if including these augmentations into the EoT process of some unlearnable example generators [6] (details in Appendix Sec. C.1). In this case, we propose the complete ST training pipeline. In step 1, we implement progressive staged training with augmentation CG to train a model. In step 2, we fine-tune the model of step 1 with augmentation CG. With this ST training pipeline, we achieve state-of-art results to defeat unlearnable samples.

Table 1: CIFAR-10 clean test accuracies (%) for natural training (NT), adversarial training (AT) and ST in different versions (ours) with various models on four unlearnable sample methods. EM-Sample is for sample-wise EM perturbations and EM-Class is for class-wise EM perturbations.

METHODS	FRAME	RESNET-18	RESNET-50	VGG-16-BN	DENSENET-121	WRN-28	WRN-34
CLEAN	NT	92.41	91.78	91.57	95.04	94.68	93.69
	NT-CG	93.2 (+0.79)	90.87 (-0.91)	91.90 (+0.33)	86.84 (-8.20)	94.63 (-0.05)	92.01 (-1.68)
	AT	88.23 (-4.18)	87.96 (-3.82)	85.32 (-6.25)	44.03 (-51.01)	78.18 (-16.50)	84.01 (-9.68)
	ST	71.97 (-20.44)	74.33 (-17.45)	56.15 (-35.42)	51.81 (-43.23)	85.08 (-9.60)	77.13 (-16.56)
	ST-CG	73.36 (-19.05)	80.65 (-11.13)	64.55 (-27.02)	55.31 (-39.73)	87.93 (-6.75)	79.07 (-14.62)
	ST-Full	93.88 (+1.47)	93.21 (+1.43)	93.01 (+1.44)	89.28 (-5.76)	95.19 (+0.51)	92.84 (-0.85)
EM-SAMPLE	NT	36.16	67.49	33.65	55.88	30.38	58.49
	NT-CG	60.03 (+24.72)	70.06 (+2.57)	64.47 (+30.82)	85.01 (+29.13)	78.48 (+48.10)	71.23 (+12.74)
	AT	88.62 (+52.46)	89.28 (+21.79)	86.28 (+52.63)	46.02 (-9.86)	71.67 (+41.29)	90.05 (+31.56)
	ST	66.03 (+29.87)	71.01 (+3.52)	56.40 (+22.75)	50.19 (-5.69)	46.87 (+16.49)	76.80 (+18.31)
	ST-CG	70.80 (+34.64)	79.45 (+11.96)	58.54 (+4.89)	57.05 (+1.17)	70.78 (+40.4)	78.31 (+19.82)
	ST-Full	87.60 (+51.44)	93.80 (+26.31)	82.48 (+48.83)	88.82 (+32.94)	88.43 (+58.05)	93.49 (+35.00)
EM-CLASS	NT	32.28	25.15	36.62	47.92	10.54	23.79
	NT-CG	78.09 (+45.81)	69.01 (+41.86)	83.47 (+46.85)	69.66 (+21.74)	60.64 (+50.10)	82.09 (+58.30)
	AT	62.09 (+29.81)	45.00 (+19.85)	40.23 (+3.61)	48.52 (+0.60)	66.43 (+55.89)	48.52 (+24.73)
	ST	55.77 (+23.49)	38.13 (+12.98)	52.68 (+16.06)	47.68 (-0.24)	31.28 (+20.74)	73.97 (+50.18)
	ST-CG	71.04 (+38.76)	78.33 (+53.18)	48.16 (+11.54)	47.34 (-0.58)	52.06 (+41.52)	79.04 (+55.25)
	ST-Full	81.61 (+49.33)	83.82 (+58.67)	86.72 (+50.10)	75.72 (+27.80)	70.73 (+60.19)	85.54 (+61.75)
REM	NT	21.86	25.30	44.19	32.28	26.43	20.37
	NT-CG	45.62 (+23.76)	44.59 (+19.29)	35.82 (-8.37)	67.09 (+34.81)	70.15 (+43.72)	47.4 (+27.03)
	AT	48.16 (+26.3)	40.65 (+15.35)	65.23 (+21.04)	32.04 (-0.24)	26.92 (+0.49)	48.39 (+28.02)
	ST	68.32 (+46.46)	56.71 (+31.41)	49.79 (+5.60)	40.34 (+8.06)	42.75 (+16.32)	74.62 (+54.25)
	ST-CG	74.69 (+52.83)	61.72 (+36.42)	52.08 (+7.89)	40.82 (+8.54)	70.53 (+44.10)	79.48 (+59.11)
	ST-Full	80.83 (+58.97)	83.09 (+57.79)	75.08 (+30.89)	72.34 (+40.06)	77.93 (+51.50)	81.88 (+61.51)
SP	NT	24.08	26.21	28.45	32.29	24.98	25.73
	NT-CG	82.94 (+58.86)	71.88 (+45.67)	82.16 (+53.71)	65.00 (+32.71)	84.66 (+59.68)	83.40 (+57.67)
	AT	22.21 (-1.87)	52.02 (+25.81)	61.12 (+32.67)	47.63 (+15.34)	58.26 (+33.28)	64.41 (+38.68)
	ST	52.52 (+28.44)	37.27 (+11.06)	49.06 (+20.61)	45.84 (+13.55)	37.43 (+12.45)	44.87 (+19.14)
	ST-CG	68.77 (+44.69)	76.09 (+49.88)	61.19 (+32.74)	50.68 (+18.39)	82.12 (+57.14)	76.00 (+50.27)
	ST-Full	81.38 (+57.30)	80.20 (+53.99)	85.16 (+56.71)	69.35 (+37.06)	88.94 (+63.96)	84.32 (+58.59)
OPS	NT	21.71	19.20	17.25	25.01	31.67	19.69
	NT-CG	51.95 (+30.24)	42.88 (+23.68)	41.58 (+24.33)	42.63 (+17.62)	60.13 (+28.46)	51.51 (+31.82)
	AT	21.08 (-0.63)	15.2 (-4.00)	18.6 (+1.35)	32.14 (+7.13)	48.19 (+16.52)	47.75 (+28.06)
	ST	49.79 (+28.08)	74.94 (+55.74)	42.2 (+24.95)	48.97 (+23.96)	47.02 (+15.35)	70.39 (+50.70)
	ST-CG	69.71 (+48.00)	71.41 (+52.21)	56.21 (+38.96)	56.11 (+31.10)	69.40 (+37.73)	73.77 (+54.08)
	ST-Full	57.87 (+36.16)	53.67 (+34.47)	52.2 (+34.95)	52.29 (+27.28)	61.42 (+29.75)	55.73 (+36.04)

4 Experiments

4.1 Experimental Setups

Datasets and model architectures. Three benchmarks, CIFAR-10, CIFAR-100 [10], and ImageNet-mini, a subset of the first 100 classes in ImageNet [17], are used in our experiments, which is consistent with previous works of unlearnable sample [9; 6; 26]. We demonstrate the effectiveness of ST with various model architectures including ResNet-18, ResNet-50 [7], WideResNet-28-10 (WRN-28), WideResNet-34-10 (WRN-34) [28], VGG-16-BN [19], and DenseNet-121 [8].

Unlearnable samples. Four state-of-the-art unlearnable samples generation methods are used: Error-Minimizing perturbation (EM) [9], Robust-Error-Minimizing perturbation (REM) [6], Synthetic Perturbation (SP) [26], and One-Pixel Shortcut (OPS) [24]. We set the ℓ_∞ bound $\|\delta\|_\infty < \epsilon = \frac{8}{255}$ for EM, REM, and SP to perturb image as much as possible without human perception. For other hyper-parameters, we follow the default settings according to their official codebases.

Training methods. To show our effectiveness, we compare the natural training method with 3 different settings of ST (as summarized in Table 3). We also adopt adversarial training (AT) with a bound of $\ell_\infty \leq \frac{4}{255}$ as the baseline, since REM using $\frac{4}{255}$ as the bound. Specifically, we implement ST with α set to 25% and γ set to 2.6×10^{-4} . We use a subset of the training dataset, D^s , containing 1000 samples for CIFAR-10 (each class contains 100 samples) and 5000 samples for CIFAR-100, ImageNet-mini (each class contains 50 samples) as the validation set to calculate the *ACM* metric during staged training. More training details will be found in Appendix Sec. A.

Table 3: Notions of different training methods, where NT denotes "natural training" which is our baseline, ST denotes our "staged training".

	NT	NT-CG	ST	ST-CG	ST-Full
Learning rate adjustment	-	-	✓	✓	✓
Augmentation CG	×	✓	×	✓	✓
Fine-tuning with CG	-	×	×	×	✓

Table 2: CIFAR-100 clean test accuracies (%) for natural training (NT), adversarial training (AT) and ST in different versions (ours) with various models on four unlearnable sample methods. EM-Sample is for sample-wise EM perturbations and EM-Class is for class-wise EM perturbations.

METHODS	FRAME	RESNET-18	RESNET-50	VGG-16-BN	DENSENET-121	WRN-28	WRN-34
CLEAN	NT	70.77	73.69	67.27	61.99	77.31	71.28
	NT-CG	73.11 (+2.34)	72.08 (-1.61)	68.68 (+1.41)	59.69 (-2.3)	76.12 (-1.19)	74.22 (+2.94)
	AT	61.50 (-9.27)	65.81 (-7.88)	56.59 (-10.68)	28.23 (-33.76)	48.72 (-28.59)	64.01 (-7.27)
	ST	44.18 (-26.59)	53.9 (-19.79)	37.56 (-29.71)	29.46 (-32.53)	60.12 (-17.19)	50.81 (-20.47)
	ST-CG	49.45 (-21.32)	51.67 (-22.02)	39.39 (-27.88)	38.66 (-23.33)	57.04 (-20.27)	52.88 (-18.40)
	ST-Full	70.45 (-0.32)	72.45 (-1.24)	71.39 (+4.12)	62.64 (+0.65)	77.64 (+0.33)	70.94 (-0.34)
EM-SAMPLE	NT	32.19	64.84	33.50	42.86	17.35	44.22
	NT-CG	60.66 (+28.47)	72.33 (+37.49)	68.04 (+34.54)	59.96 (+17.10)	32.70 (+15.35)	69.11 (+24.89)
	AT	64.17 (+31.98)	66.43 (+31.59)	56.96 (+23.44)	26.51 (-16.35)	46.15 (+28.8)	68.27 (+24.05)
	ST	42.04 (+9.85)	51.74 (+16.90)	41.28 (+7.78)	31.67 (-11.19)	51.02 (+33.67)	51.82 (+7.60)
	ST-CG	50.86 (+18.67)	55.54 (+20.7)	34.68 (+1.18)	31.92 (-10.96)	59.42 (+42.07)	56.06 (+11.84)
	ST-Full	62.73 (+30.54)	72.57 (+37.73)	70.73 (+37.23)	62.56 (+19.7)	42.64 (+25.29)	69.78 (+25.56)
EM-CLASS	NT	9.39	11.56	11.86	34.54	7.80	13.45
	NT-CG	34.22 (+24.83)	72.00 (+60.44)	68.44 (+56.58)	58.20 (+23.66)	42.50 (+34.70)	52.94 (+39.49)
	AT	36.65 (+27.26)	28.12 (+16.56)	33.77 (+21.91)	28.42 (-6.12)	47.64 (+39.84)	52.43 (+38.98)
	ST	34.36 (+24.97)	46.75 (+35.19)	38.98 (+27.12)	30.52 (-4.02)	49.93 (+42.13)	48.86 (+35.41)
	ST-CG	48.64 (+39.25)	57.68 (+46.12)	34.59 (+22.73)	37.87 (+3.33)	60.21 (+52.41)	53.21 (+39.76)
	ST-Full	48.88 (+39.49)	71.77 (+60.21)	71.30 (+59.44)	60.54 (+26.00)	50.09 (+42.29)	54.02 (+40.57)
REM	NT	8.71	17.28	13.51	16.04	8.83	10.65
	NT-CG	47.04 (+38.33)	41.43 (+24.15)	31.30 (+17.79)	34.52 (+18.48)	45.61 (+36.78)	47.44 (+36.79)
	AT	27.10 (+18.39)	26.03 (+8.75)	48.85 (+35.34)	21.18 (+5.14)	39.25 (+30.42)	25.04 (+14.39)
	ST	47.91 (+39.20)	38.10 (+20.82)	28.79 (+15.28)	21.34 (+5.30)	39.87 (+31.04)	48.26 (+37.61)
	ST-CG	51.13 (+42.42)	40.38 (+23.10)	23.81 (+10.30)	18.68 (+2.64)	56.01 (+47.18)	54.42 (+43.77)
	ST-Full	55.95 (+47.24)	57.66 (+40.38)	37.85 (+24.34)	37.37 (+21.33)	60.39 (+51.56)	59.58 (+48.93)
SP	NT	12.15	15.5	18.12	19.70	19.57	13.29
	NT-CG	58.94 (+46.79)	51.09 (+35.59)	62.45 (+44.33)	44.50 (+24.80)	60.96 (+41.39)	51.82 (+38.53)
	AT	24.81 (+12.66)	29.84 (+14.34)	28.71 (+10.59)	23.19 (+3.49)	39.11 (+19.54)	43.09 (+29.80)
	ST	20.84 (+8.69)	17.43 (+1.93)	25.08 (+6.96)	27.05 (+7.35)	27.82 (+8.25)	16.18 (+2.89)
	ST-CG	46.39 (+34.24)	48.15 (+32.65)	35.30 (+17.18)	32.45 (+12.75)	50.11 (+30.54)	48.50 (+35.21)
	ST-Full	53.93 (+41.78)	50.41 (+34.91)	64.89 (+46.91)	40.81 (+21.11)	62.52 (+42.95)	59.13 (+45.84)
OPS	NT	13.93	12.21	8.90	12.85	14.55	11.34
	NT-CG	30.86 (+16.93)	18.79 (+6.58)	12.97 (+4.07)	20.43 (+7.58)	34.11 (+19.56)	30.31 (+18.97)
	AT	10.85 (-3.08)	17.07 (4.86)	10.17 (+1.27)	11.15 (-1.7)	21.86 (+7.31)	24.82 (+13.48)
	ST	32.06 (+18.13)	52.78 (+40.57)	34.77 (+25.87)	25.98 (+13.13)	29.85 (+15.30)	51.48 (+40.14)
	ST-CG	45.86 (+31.93)	49.31 (+37.10)	24.34 (+15.44)	25.86 (+13.01)	46.25 (+31.7)	48.72 (+37.38)
	ST-Full	37.79 (+23.86)	33.73 (+21.52)	13.31 (+4.41)	23.56 (+10.71)	37.59 (+23.04)	42.52 (+31.18)

Learning Effectiveness. Table 1 and Table 2 show the clean test accuracy of models on CIFAR-10 and CIFAR-100 after being trained with different methods on the perturbed training data. As a pioneering method, EM-Sample and EM-Class perturbations have limited data protection capabilities, while methods on improving it like REM and OPS show that the natural training method cannot work well on perturbed data, most of which are less than 33% on CIFAR-10 and 20% on CIFAR-100. Adversarial training (AT) works well on EM-Sample, EM-Class and SP perturbations. However, AT is still trivial compared with our ST training pipeline. Especially, ST-Full trained ResNet-50 gets 93.80% on EM-Sample perturbed CIFAR-10, and ST-Full trained VGG-16-BN gets 71.30% on EM-Class perturbed CIFAR-100. Meanwhile, ST training pipeline works effectively on clean data as well as normal training.

Furthermore, to confirm the effectiveness of high-resolution images, we implement the ST training pipeline on ImageNet-mini. As shown in Table 4, ST works well on four perturbed data (especially, ST improves ResNet-18 from 11.10% to 63.34% on SP and DenseNet-121 from 6.58% to 48.70% on EM-Sample). CG augmentation makes supplement the performance of ST, which ST-CG achieves a good boost to ST. Meanwhile, ST-Full works perfectly on REM and SP perturbation. However, it has a decreased accuracy on EM-Sample and EM-Class with ResNet-18. This is because the protection of perturbation on high-resolution images is much stronger (an example: 32.38% for a naturally trained ResNet-18 on EM-Class perturbed CIFAR-10 in Table 1 while 3.95% for a naturally trained ResNet-18 on EM-Class perturbed ImageNet-mini in Table 4).

4.2 Analysis

ST helps to avoid overfitting. We further illustrate how the ST framework help to avoid overfitting. We first train a model on REM perturbed data. When this model has a tendency to overfitting ($ACM > \gamma$), we either keep ST training (orange lines in Fig. 5) or natural training (blue, green, red lines in Fig. 5). The results show that ST performs well in defeating unlearnable samples. Without the learning rate adjustment algorithm, the model will fall back to overfitting, similar to natural training, which shows the necessity of learning rate adjustment. We plot the channel-wise activation

Table 4: ImageNet-mini clean test accuracies (%) for natural training (NT), adversarial training (AT), and our ST in different settings over various unlearnable sample methods. EM-Sample is for sample-wise EM perturbations and EM-Class is for class-wise EM perturbations.

METHOD	MODEL	NT	NT-CG	AT	ST	ST-CG	ST-Full
CLEAN	RESNET-18	80.66	81.50 (+0.84)	65.73 (-14.93)	66.29 (-14.37)	71.05 (-9.61)	83.14 (+2.48)
	DENSENET-121	80.27	80.19 (-0.08)	54.25 (-26.02)	52.68 (-27.59)	53.66 (-26.61)	81.50 (+1.23)
EM-SAMPLE	RESNET-18	14.81	7.85 (-6.96)	50.05 (+35.24)	32.11 (+17.30)	57.34 (+42.53)	41.34 (+26.53)
	DENSENET-121	6.58	41.13 (+34.55)	37.15 (+30.57)	48.70 (+42.12)	52.92 (+46.34)	57.21 (+50.63)
EM-CLASS	RESNET-18	3.95	2.35 (-1.60)	50.45 (+46.50)	27.67 (+23.72)	47.77 (+43.82)	26.26 (+22.31)
	DENSENET-121	9.31	26.47 (+17.16)	39.62 (+30.31)	48.09 (+38.78)	49.84 (+40.53)	54.61 (+45.30)
REM	RESNET-18	13.74	68.29 (+54.55)	50.43 (+36.69)	43.26 (+29.52)	58.16 (+44.42)	69.36 (+55.62)
	DENSENET-121	32.00	70.82 (+38.82)	38.63 (+6.63)	41.20 (+9.2)	51.04 (+19.04)	72.54 (+40.54)
SP	RESNET-18	11.10	78.65 (+67.55)	52.05 (+40.95)	63.34 (+52.24)	61.32 (+50.22)	79.48 (+68.38)
	DENSENET-121	12.58	79.07 (+66.49)	38.29 (+25.71)	48.38 (+35.80)	50.20 (+37.62)	80.30 (+67.72)

magnitudes of different layers (details in Appendix Sec. C.2), which verifies that ST successfully resists overfitting. We also draw the loss landscape [13] of a model natural trained and ST trained on unlearnable samples, which shows that unlearnable samples traps the model in an overfitting way (details in Appendix Sec. C.7).

Hyperparameter analysis. We analyzed the sensitivity of hyperparameter γ and β (details in Appendix Sec. C.3). $2.6e^{-4}$ is a suitable value for γ , and $\frac{1}{4}$ is a suitable value for β .

Different protection percentages. There is a more realistic learning scenario, where only a part of the data are protected by the defensive noise, while the others are clean. We used various unlearnable method perturbed CIFAR-10 and CIFAR-100 with different mixing ratios. The protection percentage (ratio) represents the proportion of unlearnable samples to all samples (details and results can be found in Appendix Sec. C.4). ST-Full has exceptional performance on all protection percentage (especially on protection percentage 1.0), which reflects the reliability of our method on mixed samples.

Comparison with general counter-overfitting methods. We have also verified the efficiency of different counter-overfitting methods to naturally train a ResNet-18 on REM perturbed CIFAR-10 in Table. 5 (details in Appendix Sec. C.5). The results reflect that ST beats these counter-overfitting methods and defeats unlearnable samples.

Table 5: CIFAR-10 test accuracy (%) of different counter-overfitting methods. WD for weight-decay

FRAME	CUTOUT [4]	MIXUP [29]	CUTMIX [27]	AUTO-AUGMENT [2]	GAUSSIAN-FILTER	DROP-OUT [20]
TEST ACC.	21.66	11.24	10.34	28.12	15.95	25.08
FRAME	WD [11] (10^{-4})	WD (10^{-3})	WD (10^{-2})	ℓ_∞ AT	ST	ST-FULL
TEST ACC.	23.51	21.99	21.71	48.16	68.32	80.83

5 Conclusion

In this paper, we study the mechanism of the open-source data protection method, unlearnable samples, which provide “shortcuts” for models by injecting imperceptible perturbations into the training data, causing it typically to ignore correct semantic features and learn incorrect perturbation features instead. We observed that unlearnable samples mislead models into a trap of overfitting to protect the privacy of data. We propose the Activation Cluster Measurement (ACM) to quantify the overfitting degree of a model. Based on that, we propose progressive staged training (ST), a novel stage training framework to gradually slow down the learning process from shallow layers to deep layers and defeat unlearnable samples for the first time. Our ST training pipeline achieves extraordinary performance and provides a baseline for further studies on unlearnable samples.

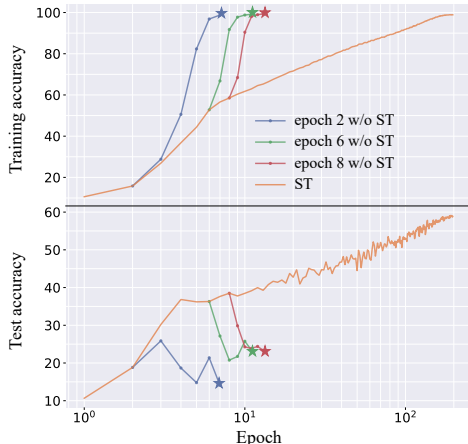


Figure 5: The training and test accuracy of a ResNet-50 ST trained on REM perturbed data (orange), and the accuracy of not implementing ST (blue, green, red).

Limitations and Broad Impacts In this work, beyond the proposed ST, we also investigate that some data augmentations, e.g., color-jitter and gray-scale (CG) [12], could promote the performance of ST. However, why these augmentations work and break the protective capability of unlearnable perturbations is not clear. We will focus on this problem in further work. Meanwhile, the breaking techniques for unlearnable samples can potentially cause negative impacts on sensitive data protection. However, by analyzing the model learning process of image semantic features and perturbation features, our work contributes important societal impacts and understanding of the rationale in this research field and provides a reliable baseline for further evaluation of unlearnable samples.

References

- [1] Battista Biggio, Blaine Nelson, and Pavel Laskov. Poisoning attacks against support vector machines. In *Proceedings of the 29th International Conference on Machine Learning, ICML 2012, Edinburgh, Scotland, UK, June 26 - July 1, 2012*. icml.cc / Omnipress, 2012.
- [2] Ekin D. Cubuk, Barret Zoph, Dandelion Mané, Vijay Vasudevan, and Quoc V. Le. Autoaugment: Learning augmentation strategies from data. In *IEEE Conference on Computer Vision and Pattern Recognition, CVPR 2019, Long Beach, CA, USA, June 16-20, 2019*, pages 113–123. Computer Vision Foundation / IEEE, 2019.
- [3] Ekin D. Cubuk, Barret Zoph, Jonathon Shlens, and Quoc V. Le. Randaugment: Practical automated data augmentation with a reduced search space. In *2020 IEEE/CVF Conference on Computer Vision and Pattern Recognition, CVPR Workshops 2020, Seattle, WA, USA, June 14-19, 2020*, pages 3008–3017. Computer Vision Foundation / IEEE, 2020.
- [4] Terrance DeVries and Graham W Taylor. Improved regularization of convolutional neural networks with cutout. *arXiv preprint arXiv:1708.04552*, 2017.
- [5] Liam Fowl, Micah Goldblum, Ping-yeh Chiang, Jonas Geiping, Wojciech Czaja, and Tom Goldstein. Adversarial examples make strong poisons. In Marc’Aurelio Ranzato, Alina Beygelzimer, Yann N. Dauphin, Percy Liang, and Jennifer Wortman Vaughan, editors, *Advances in Neural Information Processing Systems 34: Annual Conference on Neural Information Processing Systems 2021, NeurIPS 2021, December 6-14, 2021, virtual*, pages 30339–30351, 2021.
- [6] Shaopeng Fu, Fengxiang He, Yang Liu, Li Shen, and Dacheng Tao. Robust unlearnable examples: Protecting data privacy against adversarial learning. In *The Tenth International Conference on Learning Representations, ICLR 2022, Virtual Event, April 25-29, 2022*. OpenReview.net, 2022.
- [7] Kaiming He, Xiangyu Zhang, Shaoqing Ren, and Jian Sun. Deep residual learning for image recognition. In *2016 IEEE Conference on Computer Vision and Pattern Recognition, CVPR 2016, Las Vegas, NV, USA, June 27-30, 2016*, pages 770–778. IEEE Computer Society, 2016.
- [8] Gao Huang, Zhuang Liu, Laurens van der Maaten, and Kilian Q. Weinberger. Densely connected convolutional networks. In *2017 IEEE Conference on Computer Vision and Pattern Recognition, CVPR 2017, Honolulu, HI, USA, July 21-26, 2017*, pages 2261–2269. IEEE Computer Society, 2017.
- [9] Hanxun Huang, Xingjun Ma, Sarah Monazam Erfani, James Bailey, and Yisen Wang. Unlearnable examples: Making personal data unexploitable. In *9th International Conference on Learning Representations, ICLR 2021, Virtual Event, Austria, May 3-7, 2021*. OpenReview.net, 2021.
- [10] Alex Krizhevsky, Geoffrey Hinton, et al. Learning multiple layers of features from tiny images. 2009.
- [11] Anders Krogh and John A. Hertz. A simple weight decay can improve generalization. In John E. Moody, Stephen Jose Hanson, and Richard Lippmann, editors, *Advances in Neural Information Processing Systems 4, [NIPS Conference, Denver, Colorado, USA, December 2-5, 1991]*, pages 950–957. Morgan Kaufmann, 1991.

- [12] Michael Laskin, Kimin Lee, Adam Stooke, Lerrel Pinto, Pieter Abbeel, and Aravind Srinivas. Reinforcement learning with augmented data. In Hugo Larochelle, Marc’Aurelio Ranzato, Raia Hadsell, Maria-Florina Balcan, and Hsuan-Tien Lin, editors, *Advances in Neural Information Processing Systems 33: Annual Conference on Neural Information Processing Systems 2020, NeurIPS 2020, December 6-12, 2020, virtual*, 2020.
- [13] Hao Li, Zheng Xu, Gavin Taylor, Christoph Studer, and Tom Goldstein. Visualizing the loss landscape of neural nets. In Samy Bengio, Hanna M. Wallach, Hugo Larochelle, Kristen Grauman, Nicolò Cesa-Bianchi, and Roman Garnett, editors, *Advances in Neural Information Processing Systems 31: Annual Conference on Neural Information Processing Systems 2018, NeurIPS 2018, December 3-8, 2018, Montréal, Canada*, pages 6391–6401, 2018.
- [14] Ilya Loshchilov and Frank Hutter. SGDR: stochastic gradient descent with warm restarts. In *5th International Conference on Learning Representations, ICLR 2017, Toulon, France, April 24-26, 2017, Conference Track Proceedings*. OpenReview.net, 2017.
- [15] Dhruv Mahajan, Ross B. Girshick, Vignesh Ramanathan, Kaiming He, Manohar Paluri, Yixuan Li, Ashwin Bharambe, and Laurens van der Maaten. Exploring the limits of weakly supervised pretraining. In Vittorio Ferrari, Martial Hebert, Cristian Sminchisescu, and Yair Weiss, editors, *Computer Vision - ECCV 2018 - 15th European Conference, Munich, Germany, September 8-14, 2018, Proceedings, Part II*, volume 11206 of *Lecture Notes in Computer Science*, pages 185–201. Springer, 2018.
- [16] Jie Ren, Han Xu, Yuxuan Wan, Xingjun Ma, Lichao Sun, and Jiliang Tang. Transferable unlearnable examples. *arXiv preprint arXiv:2210.10114*, 2022.
- [17] Olga Russakovsky, Jia Deng, Hao Su, Jonathan Krause, Sanjeev Satheesh, Sean Ma, Zhiheng Huang, Andrej Karpathy, Aditya Khosla, Michael S. Bernstein, Alexander C. Berg, and Li Fei-Fei. Imagenet large scale visual recognition challenge. *Int. J. Comput. Vis.*, 115(3):211–252, 2015.
- [18] Juncheng Shen, Xiaolei Zhu, and De Ma. Tensorclog: An imperceptible poisoning attack on deep neural network applications. *IEEE Access*, 7:41498–41506, 2019.
- [19] Karen Simonyan and Andrew Zisserman. Very deep convolutional networks for large-scale image recognition. In Yoshua Bengio and Yann LeCun, editors, *3rd International Conference on Learning Representations, ICLR 2015, San Diego, CA, USA, May 7-9, 2015, Conference Track Proceedings*, 2015.
- [20] Nitish Srivastava, Geoffrey E. Hinton, Alex Krizhevsky, Ilya Sutskever, and Ruslan Salakhutdinov. Dropout: a simple way to prevent neural networks from overfitting. *J. Mach. Learn. Res.*, 15(1):1929–1958, 2014.
- [21] Chen Sun, Abhinav Shrivastava, Saurabh Singh, and Abhinav Gupta. Revisiting unreasonable effectiveness of data in deep learning era. In *IEEE International Conference on Computer Vision, ICCV 2017, Venice, Italy, October 22-29, 2017*, pages 843–852. IEEE Computer Society, 2017.
- [22] Ilya Sutskever, James Martens, George E. Dahl, and Geoffrey E. Hinton. On the importance of initialization and momentum in deep learning. In *Proceedings of the 30th International Conference on Machine Learning, ICML 2013, Atlanta, GA, USA, 16-21 June 2013*, volume 28 of *JMLR Workshop and Conference Proceedings*, pages 1139–1147. JMLR.org, 2013.
- [23] Laurens Van der Maaten and Geoffrey Hinton. Visualizing data using t-sne. *Journal of machine learning research*, 9(11), 2008.
- [24] Shutong Wu, Sizhe Chen, Cihang Xie, and Xiaolin Huang. One-pixel shortcut: on the learning preference of deep neural networks. *arXiv preprint arXiv:2205.12141*, 2022.
- [25] Huang Xiao, Battista Biggio, Gavin Brown, Giorgio Fumera, Claudia Eckert, and Fabio Roli. Is feature selection secure against training data poisoning? In Francis R. Bach and David M. Blei, editors, *Proceedings of the 32nd International Conference on Machine Learning, ICML 2015, Lille, France, 6-11 July 2015*, volume 37 of *JMLR Workshop and Conference Proceedings*, pages 1689–1698. JMLR.org, 2015.

- [26] Da Yu, Huishuai Zhang, Wei Chen, Jian Yin, and Tie-Yan Liu. Availability attacks create shortcuts. In Aidong Zhang and Huzefa Rangwala, editors, *KDD '22: The 28th ACM SIGKDD Conference on Knowledge Discovery and Data Mining, Washington, DC, USA, August 14 - 18, 2022*, pages 2367–2376. ACM, 2022.
- [27] Sangdoon Yun, Dongyoon Han, Sanghyuk Chun, Seong Joon Oh, Youngjoon Yoo, and Junsuk Choe. Cutmix: Regularization strategy to train strong classifiers with localizable features. In *2019 IEEE/CVF International Conference on Computer Vision, ICCV 2019, Seoul, Korea (South), October 27 - November 2, 2019*, pages 6022–6031. IEEE, 2019.
- [28] Sergey Zagoruyko and Nikos Komodakis. Wide residual networks. In Richard C. Wilson, Edwin R. Hancock, and William A. P. Smith, editors, *Proceedings of the British Machine Vision Conference 2016, BMVC 2016, York, UK, September 19-22, 2016*. BMVA Press, 2016.
- [29] Hongyi Zhang, Moustapha Cissé, Yann N. Dauphin, and David Lopez-Paz. mixup: Beyond empirical risk minimization. In *6th International Conference on Learning Representations, ICLR 2018, Vancouver, BC, Canada, April 30 - May 3, 2018, Conference Track Proceedings*. OpenReview.net, 2018.

A Experimental Details

A.1 Data Augmentations

Crop and flip. Following previous work on unlearnable samples (EM, REM and SP), we perform random flipping on the image in all experiments. Then, we randomly crop the image to 32×32 size for CIFAR-10 and CIFAR-100 and 224×224 size for ImageNet-mini.

Color-jitter and gray-scale Color-jitter randomly changes the brightness, contrast, saturation, and hue of an image. Gray-scale randomly converts an image to a grayscale one. Following traditional data augmentation methods in deep learning, we perform color-jitter on images with 80% probability and gray-scale with 20% probability.

Cutout. Cutout is an augmentation to randomly mask some areas of images, and we set the mask size to 16.

Guassain-filter. Guassain-filter smooths and blur an image. We implement Guassain-filter with σ set to 1.5 and kernel-size set to 5.

A.2 Training

For NT, we use the SGD optimizer accompanied by the cosine learning rate decay, with momentum set to 0.9, weight decay set to 10^{-4} , and learning rate set to 0.1. For AT, we use the SGD optimizer accompanied by the cosine learning rate decay, with momentum set to 0.9, weight decay set to 10^{-4} , and learning rate set to 0.1. For ST series, we use the SGD optimizer accompanied by the cosine learning rate decay, with momentum set to 0.9, weight decay set to 10^{-4} , and learning rate set to 0.1 for ST and 0.2 for ST-CG. For fine-tuning with CG, we use the SGD optimizer accompanied by the cosine learning rate decay, with momentum set to 0.9, weight decay set to 10^{-4} , and learning rate set to 0.3. All experiments are conducted on 8 GPU (NVIDIA[®] Tesla[®] A100[®]). We set other hyperparameters to the default value in the open-sourced codes of EM², REM³, SP⁴, OPS⁵.

B Observations

B.1 Observations for Insight 1

We also show the learning process of a ResNet-50 and a WRN34-10 separately on unlearnable CIFAR-10 and CIFAR-100 in Fig. 6. Both the training accuracy and test accuracy increase at the first several epochs, indicating that the model learned the correct image features. However, with training goes on, the training accuracy increases sharply, while the test accuracy significantly decreases, indicating the model is overfitting and trapped in the perturbation feature learning. These observations provide direct evidence for our insight 1.

B.2 Observations for Insight 2

We also show the learning process of a ResNet-50 and a WRN34-10 separately on unlearnable CIFAR-10 and CIFAR-100. As shown in Fig. 7, M^S performs better test data, which proves that shallow layers are capable of learning the correct features at the beginning of the training (like M^S). However, when shallow layers are overfitting, even if deep layers are in the right state (like M^D), shallow layers will pass wrong activation and corrupt deep layers to an overfitting way. These observations provide direct evidence for our insight 2.

²<https://github.com/HanxunH/Unlearnable-Examples>

³<https://github.com/fshp971/robust-unlearnable-examples>

⁴<https://github.com/dayu11/Availability-Attacks-Create-Shortcuts>

⁵<https://openreview.net/forum?id=p7G8t5FVn2h>

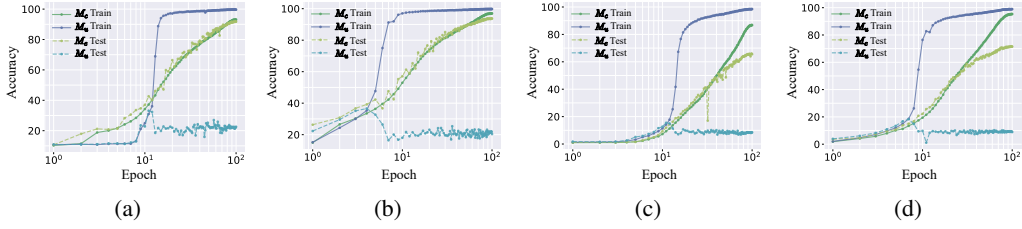


Figure 6: (a) The training and test accuracy of a ResNet-50 trained on clean CIFAR-10 (M_c) and REM perturbed CIFAR-10 (M_u). (b) The training and test accuracy of a WRN34-10 trained on clean CIFAR-10 (M_c) and perturbed CIFAR-10 (M_u). (c) The training and test accuracy of a ResNet-50 trained on clean CIFAR-100 (M_c) and REM perturbed CIFAR-10 (M_u). (d) The training and test accuracy of a WRN34-10 trained on clean CIFAR-100 (M_c) and perturbed CIFAR-100 (M_u).

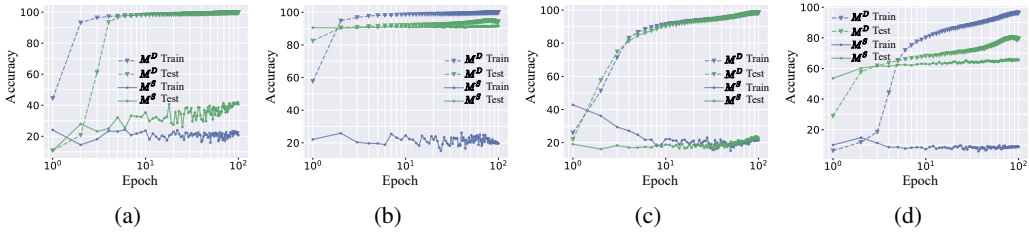


Figure 7: (a) The training and test accuracy of M^S (green) and M^D (blue) with WRN34-10 on REM perturbed CIFAR-10. (b) The training and test accuracy of M^S (green) and M^D (blue) with VGG-16-BN on REM perturbed CIFAR-10. (c) The training and test accuracy of M^S (green) and M^D (blue) with ResNet-18 on REM perturbed CIFAR-100. (d) The training and test accuracy of M^S (green) and M^D (blue) with VGG-16-BN on REM perturbed CIFAR-100.

C Ablation Study

C.1 Data Augmentation Influences

We propose composite data augmentation strategies to improve the learning effectiveness on unlearnable samples in the further step. In this section, we analyze that the CG transformed image data lowers the chance of overfitting. Such composite data augmentation can work effectively even if the augmentation strategy is white-box during generating unlearnable examples, because it is hard to build effective unlearnable examples with more complex perturbation feature space. We implement augmentation CG while generating REM perturbations, and we denote this perturbations by REM-T which generate as follows:

$$\arg \min_{\theta} \mathbb{E}_{(\mathbf{x}_i, \mathbf{y}_i)} \left[\min_{\delta_i} \max_{\sigma_i} \mathcal{L}(f_{\theta}(t(\mathbf{x}_i + \delta_i + \sigma_i)), \mathbf{y}_i) \right] \quad (8)$$

where $\|\sigma_i\|_{\infty} < \epsilon_a$, $\|\delta_i\|_{\infty} < \epsilon_u$ and t is the augmentation CG, \mathcal{L} is the loss function.

CG works well even if the augmentation strategy is white-box during generating unlearnable examples. The reason why REM-T hardly generates effective unlearnable examples is that REM-T produces much more complex perturbation feature space, hence models have less chance to be trapped in learning REM-T features. To validate this statement, we introduce the experiments as follows. We modified a REM perturbations training dataset which adds REM vanilla perturbations to newly generating perturbations. Then, we trained a ResNet-18 model on this mixed-perturbation dataset, and separately tested this model on REM vanilla perturbations (REM) and REM-T perturbations (REM-T). The training dataset contains 45000 mixed-perturbation samples, and each testing dataset contains 5000 perturbation samples. To prevent data leakage, the training dataset and two testing dataset have no common perturbation sample. As shown in Table 6, the accuracy of REM is 85.58% and the accuracy of REM-T is 12.36%, which reflects that REM-T features is harder than vanilla REM features and weaker on data protection. In this case, the model is "lazy" to learn REM-T features and prefers REM features.

Table 6: The different test accuracy of a ResNet-18 trained on REM and REM-T mixed-perturbation dataset.

TESTING DATASET	TEST ACC.	COMPLEXITY	DATA PROTECTION CAPABILITY
REM	85.58%	EASY TO LEARN	STRONG
REM-T	12.36%	HARD TO LEARN	WEAK

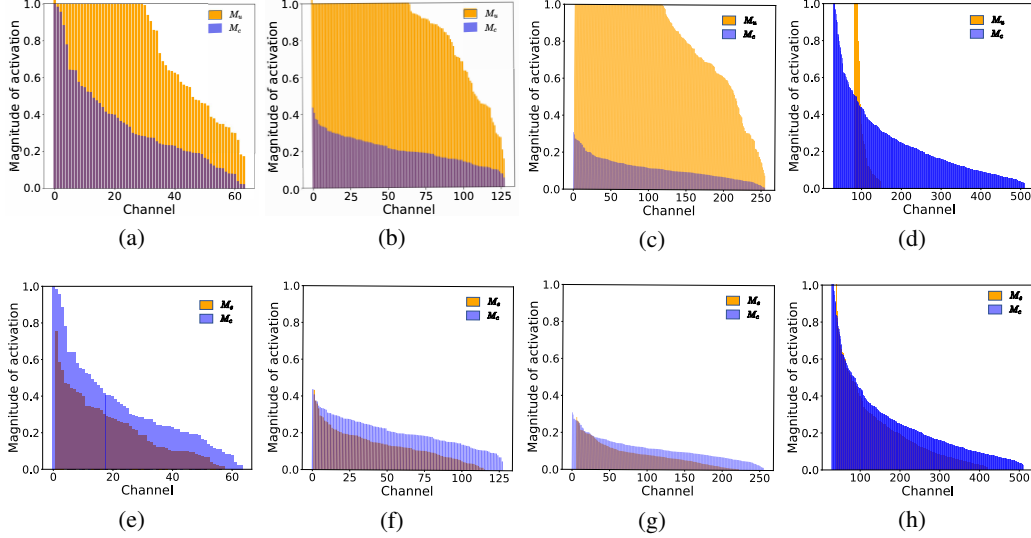


Figure 8: (a) to (d) is the channel-wise mean value of output activation form the shallow layers to the deep layers of model M_c and M_u . (e) to (h) is the channel-wise mean value of output activation form the shallow layers to the deep layers of model M_c and M_s . (a) and (e) is the output activation distribution of the second residual block layer. (b) and (f) is the output activation distribution of the fourth residual block layer. (c) and (g) is the output activation distribution of the sixth residual block layer. (d) and (h) is the output activation distribution of the residual block layer before full connection layer.

The above analysis provides irrefutable evidence of that augmentation CG makes unlearnable samples weak on data protection, even if implements CG during the generation process of unlearnable perturbations.

C.2 Channel-wise Activation Analysis

To verify the effectiveness of ST, we analyses the channel-wise activation of different layers. We natural trained a ResNet-18 model separately on clean data (M_c) and REM perturbed data (M_u). Then we ST trained a ResNet-18 on REM perturbed data (M_s). We analyses the channel-wise mean value of output activation form the shallow layers to the deep layers of model M_c , M_u and M_s , when feed them with clean data. As shown in Fig. 8, the activation distribution of M_s is similar with M_c , while the activation distribution of M_u is largely different with M_c and M_s . In this case, ST resists overfitting and leads model to a correct way indeed.

C.3 Hyperparameter Analysis

We analyzed the sensitivity of hyperparameter γ and β . As shown in Fig. 9, 2.6×10^{-4} is a suitable value for γ , and $\frac{1}{4}$ is a suitable value for β .

C.4 Different Protection Percentages

There is a more realistic learning scenario, where only a part of the data is protected by the defensive noise, while the others are clean. We used perturbed CIFAR-10 and CIFAR-100 with different mixing ratios. The protection percentage (ratio in Table 7 and Table 8) represents the proportion of unlearnable samples to all samples. As shown in Table 7 and Table 8, ST-Full has exceptional

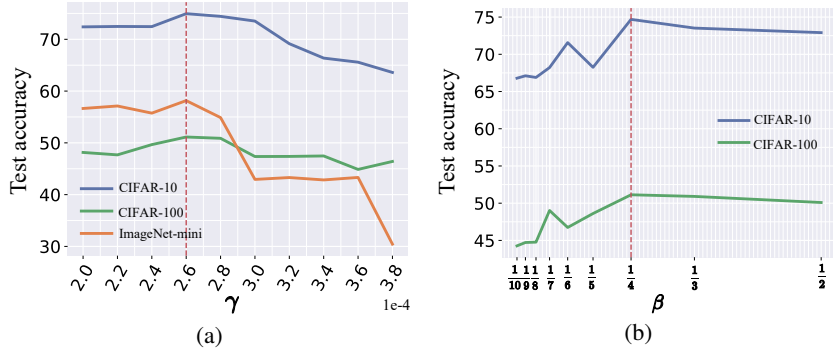


Figure 9: (a) The test accuracy of a ResNet-18 ST-CG trained on REM perturbed data. (b) The test accuracy of a ResNet-18 ST-CG trained on REM perturbed data.

performance on all protection percentages (especially on protection percentage 1.0), which reflects the reliability of our method on mixed samples.

Table 7: ResNet-18 test accuracies (%) for NT and ST trained on perturbed CIFAR-10 with different protection percentages (Ratio).

		RATIO	0	0.2	0.4	0.6	0.8	1
EM-SAMPLE	NT		92.41	93.12	92.04	90.72	83.90	36.16
	ST		71.97	73.70	71.23	72.18	72.54	66.03
	ST-CG		73.36	77.00	73.65	76.55	76.45	70.80
	ST-Full		93.88	93.93	93.70	92.82	92.86	87.60
EM-CLASS	NT		92.41	92.89	91.97	88.95	84.54	32.28
	ST		71.97	71.22	73.83	67.72	69.08	55.77
	ST-CG		73.36	72.36	75.09	76.68	73.51	71.04
	ST-Full		93.88	93.89	93.43	93.54	92.55	81.61
REM	NT		92.41	92.15	91.75	89.29	84.65	21.86
	ST		71.97	72.19	72.77	72.37	69.44	68.32
	ST-CG		73.36	74.80	71.54	74.66	74.81	74.69
	ST-Full		93.88	81.04	78.11	79.97	78.92	80.83
SP	NT		92.41	93.09	91.50	90.11	85.19	24.08
	ST		71.97	79.22	70.95	69.86	64.97	52.52
	ST-CG		73.36	76.00	74.83	73.90	72.04	68.77
	ST-Full		93.88	93.86	93.32	93.06	91.97	81.38
OPS	NT		92.41	82.45	88.26	89.68	92.02	21.71
	ST		71.97	83.11	88.94	91.57	91.06	49.79
	ST-CG		73.36	84.09	89.20	91.02	87.79	69.71
	ST-Full		93.88	85.15	90.25	92.19	92.79	57.87

C.5 Settings of general counter-overfitting methods

The data augmentations, including cutout, mixup, cutmix, auto-augment, and gaussian-filter (some implementation details in Appendix Sec. A.1), ineffectively resist unlearnable samples. Then, we implement drop-out (0.5 probability) and weight-decay (WD) from 10^{-4} to 10^{-2} , both of which cannot defeat unlearnable samples. Finally, we use adversarial training (AT) with $\ell_\infty \leq \frac{4}{255}$.

C.6 Activation t-SNE Analysis

We natural trained a ResNet-18 on clean data (M_c) and unlearnable data (M_u), and compare them with a ResNet-18 ST trained on unlearnable data (M_s). Then we drew the t-SNE cluster results of the output activation of the fourth residual block layer (Fig. 10) and the sixth residual block layer (Fig. 11) of ResNet-18. The results show that when a raw model is trained on unlearnable data, the

Table 8: ResNet-18 test accuracies (%) for NT and ST trained on perturbed CIFAR-100 with different protection percentages (Ratio).

	RATIO	0	0.2	0.4	0.6	0.8	1
EM-SAMPLE	NT	70.77	73.83	73.26	67.29	56.38	32.19
	ST	44.18	44.43	43.68	44.34	44.04	42.04
	ST-CG	49.45	49.89	49.00	50.93	52.00	50.86
	ST-Full	70.45	71.54	72.38	71.51	70.12	62.73
EM-CLASS	NT	70.77	74.86	71.83	65.86	57.69	9.39
	ST	44.18	47.87	47.91	45.89	43.77	34.36
	ST-CG	49.45	50.04	49.63	48.66	48.70	48.64
	ST-Full	70.45	71.86	71.90	69.62	67.13	48.88
REM	NT	70.77	72.75	68.91	63.81	53.57	8.71
	ST	44.18	44.41	44.02	44.49	43.65	47.91
	ST-CG	49.45	49.62	50.31	47.73	49.53	51.13
	ST-Full	70.45	56.36	55.72	54.26	55.32	55.95
SP	NT	70.77	73.68	71.37	67.55	57.88	12.15
	ST	44.18	49.07	46.77	44.84	40.50	20.84
	ST-CG	49.45	54.27	51.13	48.27	50.11	46.39
	ST-Full	70.45	71.97	70.06	71.48	68.98	53.93
OPS	NT	70.77	41.09	58.93	64.94	69.93	13.93
	ST	44.18	42.15	59.06	66.19	63.12	32.06
	ST-CG	49.45	50.18	59.75	66.18	57.57	45.86
	ST-Full	70.45	51.47	60.93	67.25	68.43	37.79

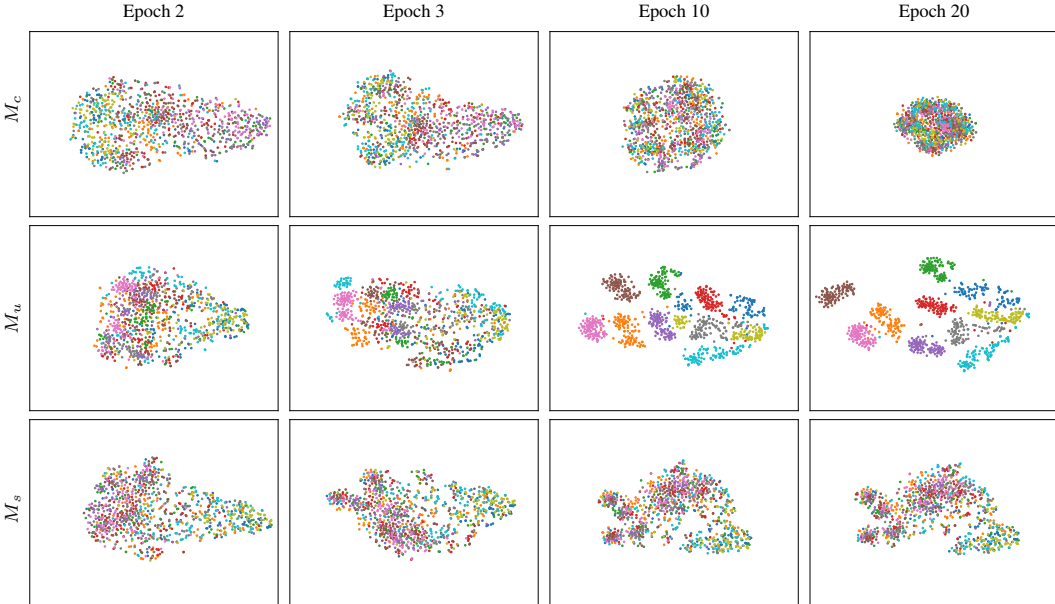


Figure 10: The t-SNE results of the fourth residual block layer output activation in different epochs. M_c is a model natural trained on clean data. M_u is a model natural trained on unlearnable data. M_s is a model ST trained on unlearnable data. Both the x-axis and the y-axis are in the range of $[-50, 50]$.

activation cluster disorder at early epochs. As training goes by, the model begins to cluster well, which is a phenomenon of overfitting. The visualization results of t-SNE also reflect the overfitting during training.

C.7 Loss Landscape

We drew the loss landscape of a natural trained ResNet-18 and a ST trained ResNet-18 on REM perturbed unlearnable data. As shown in Fig. 12, the natural trained ResNet-18 falls in a deep (dark

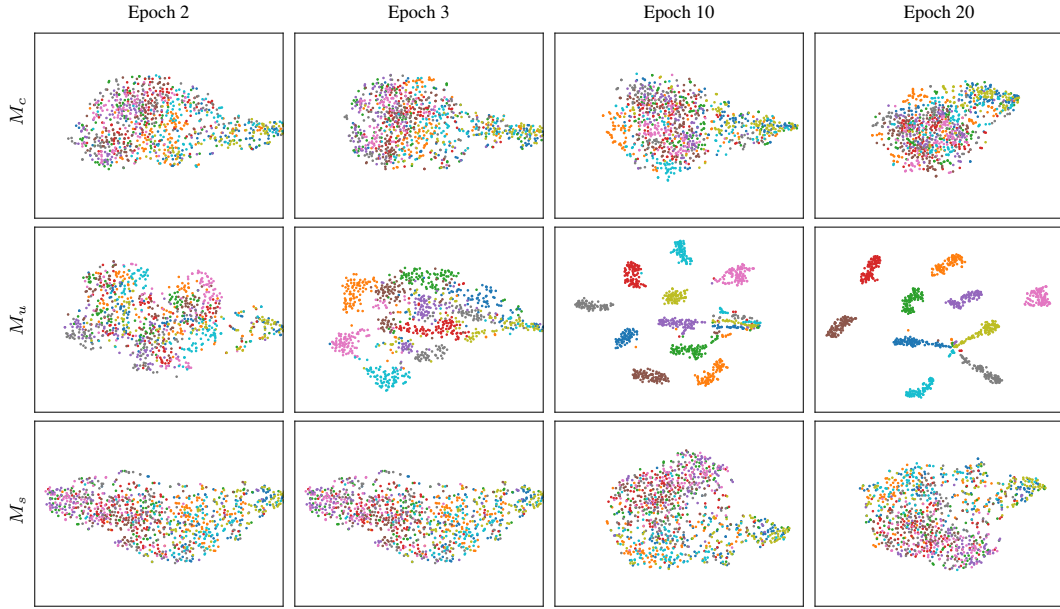


Figure 11: The t-SNE results of the sixth residual block layer output activation in different epochs. M_c is a model natural trained on clean data. M_u is a model natural trained on unlearnable data. M_s is a model ST trained on unlearnable data. Both the x-axis and the y-axis are in the range of $[-50, 50]$.

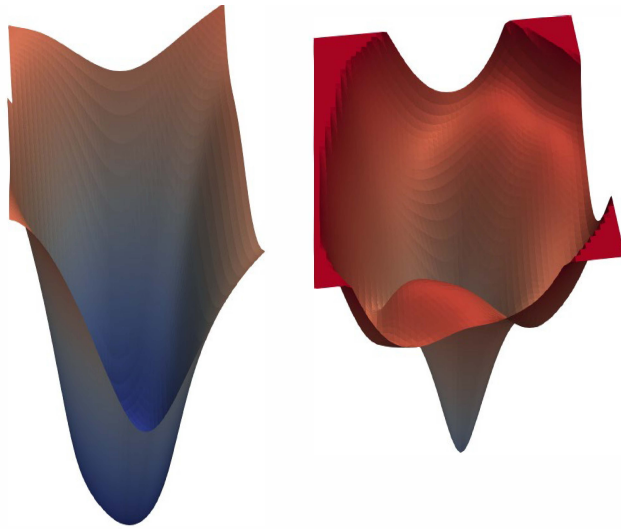


Figure 12: Loss landscape of a ResNet-18 model natural trained (left) and ST-Full (ours) trained (right) on unlearnable CIFAR-10. The natural trained model drop into a smoother and deeper trap compared with the ST-Full trained model.

blue) and smooth trap of global minimum which is hard to get out. While the ST trained ResNet-18 arrives in a shallow (light blue) and sharper local minimum compared with the previous one.